Article

Cite This: *Biomacromolecules* 2019, 20, 2694−2702

pubs.acs.org/Biomac

# Core−Shell−Shell Nanoparticles for NIR Fluorescence Imaging and NRET Swelling Reporting of Injectable or Implantable Gels

Hannah R. Shanks,*[,†] Amir H. Milani,[†] Dongdong Lu,[†] Brian R. Saunders,*[,†] Louise Carney,[†] Daman J. Adlam,[‡] Judith A. Hoyland,[‡,§] Christopher Blount,[∥,⊥] and Mark Dickinson[∥,⊥]

[†]School of Materials, University of Manchester, MSS Tower, Manchester, M13 9PL, U.K.

[‡]Division of Cell Matrix Biology and Regenerative Medicine, Faculty of Biology, Medicine and Health, University of Manchester, Oxford Road, Manchester, M13 9PT, U.K.

[§]NIHR Manchester Biomedical Research Centre, Manchester University NHS Foundation Trust, Manchester Academic Health Science Centre, Manchester, M20 2LR, U.K.

[∥]Photon Science Institute, University of Manchester, Oxford Road, Manchester, M13 9PL, U.K.

[⊥]School of Physics & Astronomy, University of Manchester, Oxford Road, Manchester, M13 9PL, U.K.

Supporting Information

**ABSTRACT:** Injectable gels that support load are desirable for restoring the mechanical properties of degenerated load-bearing tissue. As these gels become increasingly sophisticated, the need to remotely image them and monitor their swelling increases. However, imaging such gels and monitoring their swelling using noninvasive means is challenging. Here, we use a very low concentration of near-infrared (NIR) core−shell−shell (CSS) reporter nanoparticles to both image and monitor swelling changes of two load-supporting gels. The load-supporting injectable gel consisted of covalently interlinked pH-responsive microgel (MG) particles. The latter gel was not cytotoxic and is termed a doubly cross-linked microgel (DX MG). Inclusion of a complementary fluorescent dye enabled ratiometric monitoring of gel swelling changes in response to pH via nonradiative resonance energy transfer (NRET). In addition, changes in the CSS nanoparticle emission intensity provided a NIR-only method that could also be used to monitor gel swelling. The gel was able to be imaged using NIR light, after being subcutaneously injected into a tissue model. To demonstrate versatility of our approach, CSS and the dye were included within a model implantable gel (poly(acrylamide/acrylic acid)) and fluorescent detection of swelling investigated. Because the concentrations of the reporting species were too low to affect the mechanical properties, our approach to remote gel imaging and swelling monitoring has good potential for application in injectable gels and implants.

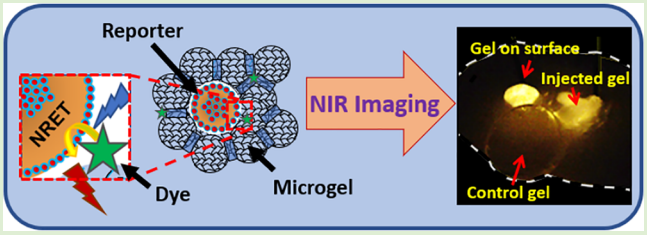


## INTRODUCTION

Injectable gels are highly desirable biomaterials that have been investigated for delivery,[1−11] tissue engineering,[12−16] and load support.[17−20] In all of these examples, the ability to noninvasively locate and monitor the gels remotely is advantageous for clinicians and researchers. However, imaging methods usually require bespoke labeling of the gel network, which may change the mechanical properties or introduce toxicity concerns and require expensive imaging instrumentation. Load supporting gels have excellent potential for intervertebral disc (IVD) repair.[17] Degeneration of the intervertebral disks, or DIVD, is a major problem that causes pain.[21−24] DIVD affects 40% of under 30 year olds and 90% of people aged 55 and over.[24] Treatment strategies for DIVD include injecting gels that form *in situ* and are sufficiently swellable, to restore the mechanical properties of degraded IVDs.[20,25,26] Here, we introduce a new and versatile approach for including reporter NIR particles within such gels that allows remote imaging and swelling changes to be monitored using low cost laboratory equipment, without the need for bespoke labeling chemistry.

Near-infrared (NIR) light deeply penetrates biological tissue[27,28] and has previously been used with gels for imaging[29] and drug delivery applications.[16] While there are examples of gels which are NIR-responsive,[30,31] there are relatively few which emit NIR light.[29] Part of the reason for the relative lack of such biomaterials is that NIR dyes usually require chemical modification to be attached to a network. As a method to circumvent this obstacle, we recently introduced particles that contain poly[2-methoxy-5-(2-ethylhexyloxy)-1,4-phenylenevinylene] (MEH-PPV) and an NIR dye silicon 2,3-naphthalocyanine bis(trihexylsilyloxide) (NIR775) in polymer dots, which were, in turn, embedded within an acrylate particle matrix.[32] These core−shell−shell (CSS) reporter particles

Received: April 3, 2019
Revised: May 31, 2019
Published: June 11, 2019




DOI: 10.1021/acs.biomac.9b00463
*Biomacromolecules* 2019, 20, 2694−2702

**Scheme 1. Preparation and Swelling of pH-Responsive Doubly Cross-Linked MG Gels (DX MG) Containing NIR Core–Shell–Shell (CSS) Reporter Particles and AF Dye**[a]

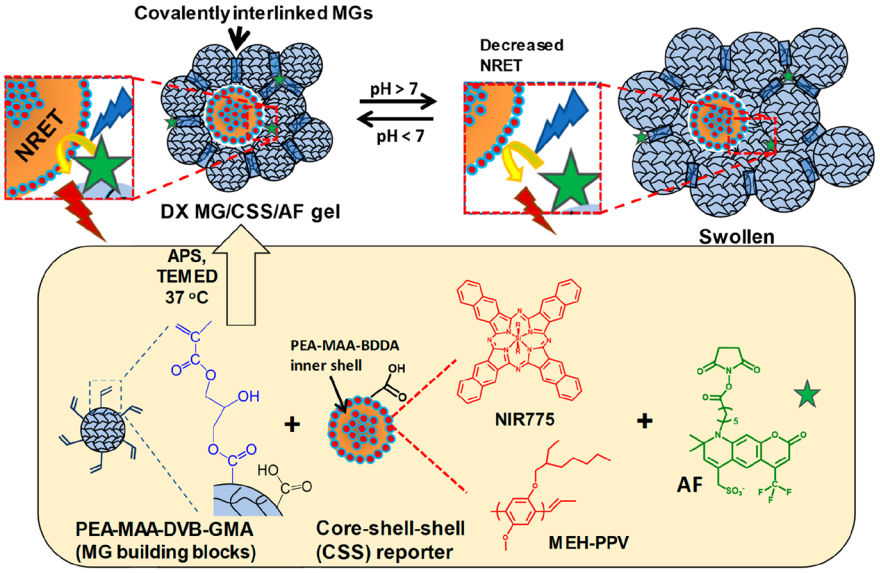


[a]EA, MAA, DVB, GMA, and BDDA are ethyl acrylate, methacrylic acid, divinyl benzene, glycidyl methacrylate, and 1,4-butanediol diacrylate, respectively. NIR775 and MEH-PPV are a near-infrared dye and poly[2-methoxy-5-(2-ethylhexyloxy)-1,4-phenylenevinylene], respectively. These two fluorophores were combined within polymer dots located within the inner and outer regions of the CSS particles, as described in ref 32.

(Scheme 1) emitted light at 775 nm and also participated in nonradiative energy transfer (NRET) in the presence of a complementary dye.[32] Here, we greatly extend our previous work by including CSS particles within an injectable gel and an implantable gel for the first time. NIR imaging of the injectable gel as well as remote swelling detection for both gels using NRET and NIR fluorescence are demonstrated.

The injectable gel used in this study is based on glycidyl methacrylate-functionalized poly(ethyl acrylate-*co*-methacrylic acid-*co*-divinylbenzene) (PEA-MAA-DVB-GMA) microgels (MGs). The latter are covalently interlinked after injection to give a hydrogel at 37 °C (Scheme 1). These gels are termed doubly cross-linked microgels (DX MGs). We stress that the term "doubly cross-linked" is well established[33] and is used to identify two types of cross-linking (intra-MG and inter-MG) of such gels and should not be confused with double network gels.[34] The MG building blocks swell when the pH approaches the particle $pK_a$.[35−43] DX MGs have been shown to be a promising system for restoring the mechanical properties of degenerated IVDs.[20] The advantage of DX MGs is that almost all of the gel construction is performed prior to injection. Here, we mixed a very small amount of CSS particles into the DX MG precursor solution prior to gel formation. We also included a dye that was complementary to the CSS particles (AF430, which is abbreviated as AF) to enable NRET for ratiometric monitoring of gel swelling changes.

NRET may occur when a donor fluorophore has an emission which overlaps the absorbance of an acceptor fluorophore.[44,45] This can cause quenching of the donor when the distance between the fluorophores is close to the Förster distance ($R_o$). The latter is the distance at which the amount of energy transferred is equal to that lost through emission.[46] $R_o$ is typically less than 10 nm. NRET is strongly dependent upon the separation distance of the fluorophores and has been used to monitor pH within biological systems.[47] NRET has also been studied for polymer dots containing MEH-PPV and NIR775.[48] In the present study, we investigate injectable DX MG/CSS/AF gels (Scheme 1). The presence of the AF dye provides a distance dependent ratiometric NRET response (via energy transfer to the CSS particles), which enables the swelling of the gels to be reported remotely. We also show that single intensity NIR emission can be used to monitor gel swelling changes.

The study begins by investigating the properties of DX MG/CSS gels. We then investigate injectable load-bearing DX MG/CSS/AF gels and their NRET behavior. The latter is shown to sensitively track the reversible pH-triggered swelling changes of the gel. The gels are also shown to have an NIR emission intensity that varies with gel swelling. The cytotoxicity of the gel is also assessed. The versatility of using NIR reporting with ratiometric detection is demonstrated by including CSS and AF within a poly(acrylamide/acrylic acid) gel, which is a model implantable gel. The study concludes with a demonstration of NIR imaging of the injectable DX MG/CSS/AF gel, when subcutaneously injected into chicken flesh. Because we demonstrate that CSS particles are a versatile and highly sensitive reporter for remote NIR imaging and monitoring of gel swelling, they should have good potential for future biomaterial applications.

## EXPERIMENTAL DETAILS

**Materials.** Ammonium persulfate 98% (APS), ethyl acrylate (EA, ≥95%), divinylbenzene (DVB, 85%), glycidyl methacrylate (GMA, ≥97.0%), acrylic acid (AA, 99%), acrylamide (AAm, ≥99%), *N*,*N*′-methylenebis(acrylamide) (mBAAm, 99%), and *N*,*N*,*N*′,*N*′-tetramethylethylenediamine (TEMED) (99%) were all purchased from Sigma-Aldrich. Alexa Fluor 430 NHS succinimidyl ester (AF) and tetrahydrofuran (THF) were purchased from ThermoFisher Scientific UK Ltd. MAA was purchased from VWR Ltd. The CSS particles were synthesized using the seed–feed emulsion polymerization method described earlier.[32] The CSS reporter particles contained MEH-PPV and NIR775 within a PEA-MAA-(1,4-butanediol diacrylate) polymer matrix (see Scheme 1). The PEA-MAA-DVB-GMA MG particles


DOI: 10.1021/acs.biomac.9b00463
Biomacromolecules 2019, 20, 2694−2702

used to construct the DX MG gels were synthesized by emulsion polymerization and then GMA-functionalized following the method previously reported.[49] All water used was ultrahigh purity and was distilled and deionized.

**Injectable DX MG/CSS/AF Gel Synthesis.** The PEA-MAA-DVB-GMA MGs were covalently interlinked to form a DX MG gel containing a small proportion of CSS particles in the presence of AF dye. Accordingly, MG dispersion (1.47 mL, 13.7 wt %) and aqueous CSS dispersion (132 $\mu$L, 2.36 × $10^{-3}$ wt % dispersion) and AF solution (132 $\mu$L, 4.7 $\mu$M) were mixed. APS solution (50 $\mu$L, 78 mM) was then added to the mixture, and this solution was added to the larger chamber of a 10:1 Medmix double-barrel syringe. A solution of NaOH (150 $\mu$L, 4.0 M) and TEMED (50 $\mu$L, 4.0 wt %) was then mixed together, with a volume ratio of 48:2, respectively, and added to the smaller chamber of the double syringe. Injection resulted in mixing of the two solutions by coextrusion, and this produced a shear-thinning physical gel due to pH-triggered MG swelling caused by the pH increase. The physical gel was then placed in an incubator at 37 °C overnight for covalent interlinking. To prepare the DX MG/CSS gels, the AF solution was replaced with the same volume of water. To prepare DX MG gels, both the AF solution and CSS dispersion were replaced with water. The pH of the as-made gels was ∼6.5.

**Implantable Poly(acrylamide/acrylic acid) Gel Synthesis.** A cross-linked poly(acrylamide/acrylic acid) gel (denoted as PAAm-AA-mBAAm) was used as a model implantable gel and prepared via free-radical copolymerization in water following the method described by Nesrinne et al.[50] AA (3.0 g, 0.042 mol) and AAm (2.0 g, 0.028 mol) were dissolved in water (7.50 g). This solution was purged with nitrogen gas for 20 min before APS (160 $\mu$L of a 0.50 g/mL solution in water), mBAAm (0.25 g, 0.0016 mol, in 16.0 mL water), and TEMED accelerator (480 $\mu$L, 0.0032 mol) were added. The monomer solution was then transferred to vials and allowed to react at room temperature for a minimum of 2 h.

**Physical Measurements.** A Malvern Zetasizer NanoZS instrument was used to measure the $z$-average diameter ($d_z$). TEM data were obtained using a Tecnai 12 Biotwin, with a Gatan 1k CCD camera. Samples were prepared using ultrathin lacey carbon and copper TEM grids (Agar Scientific), and dispersion samples were dried at room temperature. Confocal laser scanning microscopy (CLSM) images were obtained using a broadband confocal Leica TCS SP5. UV−visible spectroscopy measurements were obtained using a Hitachi U-1800 spectrophotometer. A FLS980 spectrometer from Edinburgh Instruments was used to obtain photoluminescence (PL) data. The excitation wavelength was set at 470 nm. Digital photographs of the gels were obtained using either white light or irradiation at 470 nm and a 495 nm lens filter.

Swelling studies for the gels used buffer solutions and a gravimetric method. The gels were suspended in buffer for 2 days to equilibrate. The volume swelling ratio ($Q$) of the gels was calculated using the following equation

$$Q = \rho_P\left(\left(\frac{Q_{(m)}}{\rho_S}\right) + \left(\frac{1}{\rho_P}\right)\right) - \left(\frac{\rho_P}{\rho_S}\right) \quad (1)$$

where $Q_{(m)}$ is the ratio of the swollen mass to the dry mass. The parameters $\rho_S$ and $\rho_P$ are the densities of the solvent and polymer, respectively. The latter was taken as 1.2 g/cm$^3$.

NIR imaging was achieved with an incident 470 nm laser. The sample investigated consisted of chicken breast (lean chicken breast purchased from Tesco Ltd., U.K.). A camera fitted with a filter which blocked light below 720 nm was used to take images of the samples, with an exposure time of 30 s. A DX MG/CSS/AF pregel (1.0 mL, 13.7 wt %) was prepared as described above and injected approximately 2.0 mm below the surface of the chicken breast at room temperature using a 21-gauge needle. The physical gel cured in situ to form DX MG/CSS/AF gel at room temperature.

**Cytotoxicity Experiments and Assays.** Human nucleus pulposus (NP) cells were cultured in Dulbecco's modified Eagle's medium supplemented with antibiotic/antimycotic (Sigma-Aldrich, U.K.), Glutamax, and 10% fetal bovine serum (Thermo Fisher Scientific, U.K.) within a humidified 5% $CO_2$ incubator at 37 °C. Cells were harvested by trypsinisation and seeded at a density of 5 × $10^4$ cells onto 13 mm sterile glass coverslips in 24-well culture plates. After overnight incubation, the media was replenished and toroid shaped gels, sterilized in 70% ethanol and washed with phosphate buffered saline (PBS), were introduced to the NP cell cultures. Control samples received a corresponding volume of PBS. The cells were then cultured for 72 h and live/dead assays (Thermo Fisher Scientific, U.K.) performed at each time point in duplicate according to the manufacturer's instructions. Images were obtained with an Olympus BX51 fluorescence microscope.

NP cells were cultured, harvested, and seeded at a density of 5 × $10^4$ cells per well onto 13 mm nontissue culture treated well plates containing disc shaped gels and controls ($n$ = 3) as described above. At the appropriate time point, PrestoBlue cell viability reagent was added (Thermo Fisher Scientific, U.K.) and incubated for 4 h. Absorbance values were then determined at 570 nm using a FLUOstar OMEGA plate reader.

## RESULTS AND DISCUSSION

**Injectable NIR DX MG Gels.** We prepared NIR DX MG/CSS gels by blending a small amount of CSS with PEA-MAA-DVB-GMA MG gel building blocks prior to free-radical coupling of the pendant MG vinyl groups (see Scheme 1). The NIR reporter CSS particles comprised only ∼0.001 wt % of the total polymer in the gel. The CSS particles were prepared using emulsion polymerization[32] and contained MEH-PPV and NIR775. The number-average diameter of these particles determined using TEM (Figure 1A) was 84 nm.[32] The particles had PL emission maxima at 590 and 775 nm (Figure S1A), which are due to MEH-PPV and NIR775, respectively. As discussed in detail previously,[32] MEH-PPV/NIR775 polymer dots were located at the core and outer shell of the CSS particles. The CSS particle inner shell was PEA-MAA-

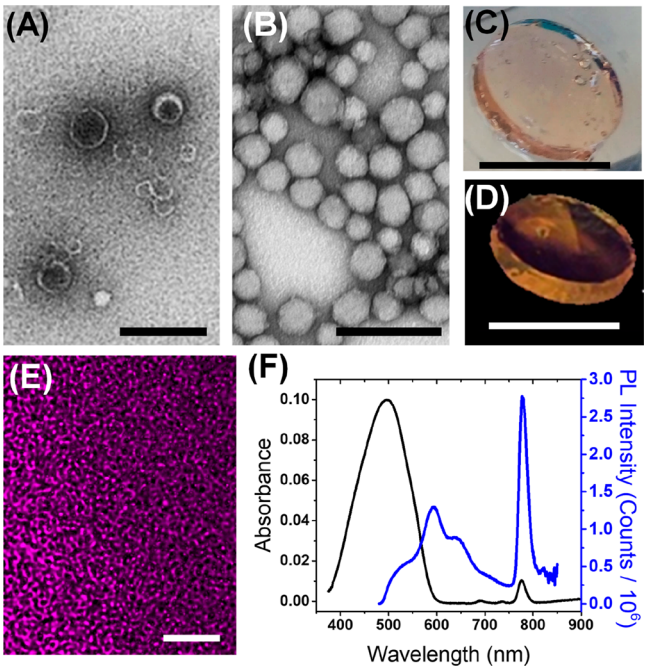


**Figure 1.** TEM images of (A) CSS particles and (B) PEA-EA-DVB-GMA MG building blocks. Scale bar: 200 nm. Photographs of DX MG/CSS gels under (C) white light and (D) 470 nm light. Scale bars: 1.0 cm. (E) CLSM $z$-stack image of the DXMG/CSS gel (excitation wavelength, $\lambda_{ex}$ = 476 nm). Scale bar: 2.0 $\mu$m. (F) UV−visible and PL emission spectra for DX MG/CSS gel.



DOI: 10.1021/acs.biomac.9b00463
Biomacromolecules 2019, 20, 2694−2702

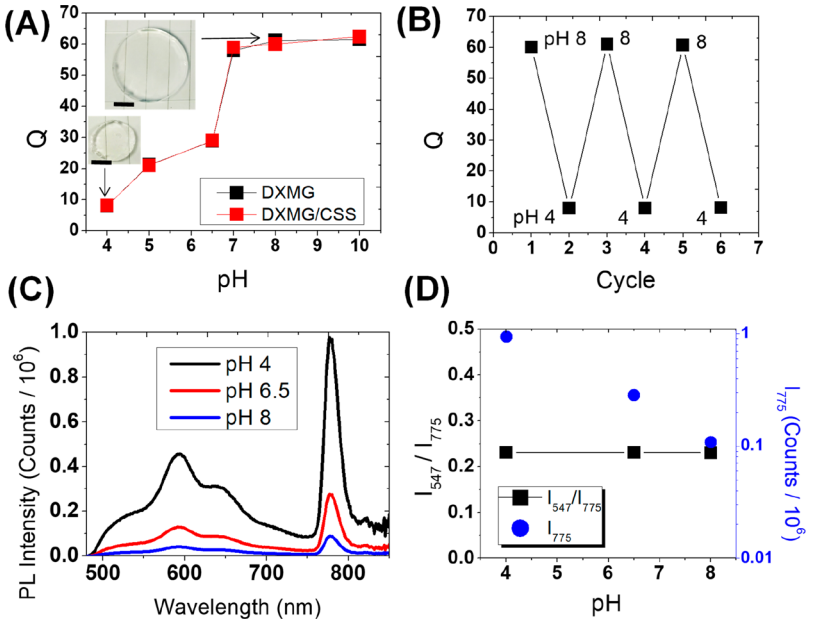


**Figure 2.** (A) Swelling ratio ($Q$) for DX MG/CSS gels with varying pH. Samples were immersed in buffers for 48 h to equilibrate prior to measurement. The inset shows images of DXMG gels. Scale bar: 6.0 mm. (B) Reversibility of DX MG/CSS gel swelling with pH switching. (C) Emission spectra for DXMG/CSS with varying pH. (D) Ratio of PL intensities measured at 547 and 775 nm ($I_{547}/I_{775}$) as well as $I_{775}$ for DXMG/CSS at different pH values.

BDDA. The PEA-EA-DVB-GMA MG building blocks used to construct the DX MG were prepared using emulsion polymerization of MAA, EA, and DVB followed by reaction with vinyl functionalization with GMA.[49] The number-average diameter of the MGs determined from TEM (Figure 1B) was 68 nm. The MGs contained 60.3% EA, 34.3 mol % MAA, 0.8 mol % DVB, and 4.6 mol % GMA from potentiometric titration data (Figure S2A). They had an apparent p$K_a$ of 6.7 and swelled strongly when the pH exceeded 6.0 (Figure S2B). The concentrated MG dispersion formed an injectable shear-thinning physical gel when the pH approached the p$K_a$ and was subsequently cured at 37 °C. The free-standing gels (Figure 1C) were orange-brown when illuminated at 470 nm (Figure 1D). A digital photograph showing the ability of the DX MG gels to be injected is shown in Figure 3A.

A representative CLSM image for the DXMG/CSS gel (Figure 1E) shows that the CSS particles were well distributed throughout the gel. This is an important advantage of the CSS particles. Our previous study showed that the CSS particles have superior dispersion stability (especially at physiological ionic strength and pH) compared to the parent MEH-PPV/NIR775 polymer dots.[32] The UV−visible absorbance and PL spectra of DXMG/CSS gel (Figure 1F) showed features due to MEH-PPV and NIR775. Indeed, the maxima in both the UV−visible absorption and PL spectra for the gel are at the same wavelengths as those in the respective spectra of the CSS particles (Figure S1A). For example, the PL emission spectrum (Figure 1F) shows the MEH-PPV and NIR775 peaks at 590 and 775 nm. The former peak for MEH-PPV was strongly red-shifted compared to the absorbance maximum (496 nm), which is a common observation for conjugated polymers which tend to have large Stokes shifts.

The DX MG/CSS gel was strongly pH-responsive due to its MAA-rich MG building blocks. Figure 2A shows that, while the gel volume swelling ratio ($Q$) had a value of 8.1 at pH 4.0, $Q$ increased to 60 at pH 8.0. Importantly, the $Q$ values of the CSS-free DX MG were indistinguishable from those for the DX MG/CSS gels. These results confirm that the CSS particles did not affect the gel network swelling. The reversibility of gel swelling was investigated using pH switching (see Figure 2B). The DX MG/CSS gel reversibly swelled between pH 4.0 and 8.0. Figure 2C shows that increasing the pH of the gel decreased the PL intensity. The strong decrease of the NIR peak PL intensity ($I_{775}$) with pH is shown in Figure 2D. This behavior is because gel swelling decreases the number of CSS particles per unit volume. This interpretation is confirmed by the fact that $I_{775}$ was pH-invariant for the parent CSS particles in dispersion (Figure S1B).

In the studies described below, we use the ratio of the PL intensities at 547 and 775 nm ($I_{547}/I_{775}$) to probe the swelling of DX MG/CSS gels containing AF. Here, we note that the $I_{547}/I_{775}$ ratio for DX MG/CSS does not change with pH (see Figure 2D). The same result was observed for the parent CSS dispersion (see Figure S1B). Such ratiometric invariance occurred because MEH-PPV and NIR775 were codeposited within hydrophobic domains of CSS that are unaffected by changes in pH or gel swelling. These results nicely exemplify the difference between single intensity PL and ratiometric measurements. The latter are less sensitive to background changes.[51] In the following section, we use both single intensity and ratiometric PL data to study DX MG/CSS/AF gel swelling.

**Injectable and Implantable NIR Gels with Built-In NRET for Monitoring Swelling.** Motivated by the NRET reporting properties of CSS particles in dispersion,[32] we hypothesized that the addition of a secondary dye with emission complementary to that of the CSS absorbance could result in swelling-dependent NRET within DXMG/CSS gels. If NRET were operative, then pH-triggered swelling could in theory alter the separation distance between the CSS and the dye, resulting in sensitive changes in energy transfer that enable ratiometric PL monitoring of swelling. In this case, both AF


DOI: 10.1021/acs.biomac.9b00463
Biomacromolecules 2019, 20, 2694−2702

and CSS particles were added to the MG pregel dispersion to prepare DX MG/CSS/AF gels (see Scheme 1). Photographs of the gels obtained under white light and 470 nm illumination are shown in Figure 3A and B, respectively. The inclusion of AF caused the emission color for the gels to become green (compare to Figure 1D).

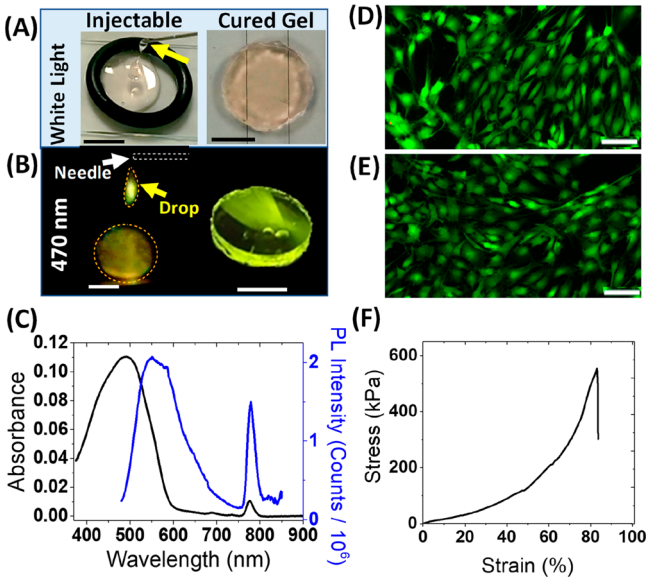


**Figure 3.** Digital photographs showing injection of the pregel used to prepare the DX MG/CSS/AF gel obtained under (A) white light and also (B) 470 nm light. The arrows highlight the point of injection. Scale bars: 5 mm. (C) UV−visible and PL spectra for DXMG/CSS/AF gels. The pH of the gel was 5.0. Live/dead images of human NP cells (D) with and (E) without DXNG/CSS/AF gel after 48 h. Green represents live cells, and red represents dead cells. Scale bars: 100 $\mu$m. (F) Uniaxial compression stress−strain data for DX MG/CSS/AF gel.

A criterion for NRET is that the PL maxima of the donor should overlap the absorbance of the acceptor.[46] Comparison of the PL and UV−visible absorbance spectra for CSS (acceptor) and AF (donor) shows that this indeed was the case (see Figure S3). The presence of AF and CSS can be seen from the UV−visible spectrum of the DX MG/CSS/AF gel as a shoulder at ∼430 nm (AF) and peak at 775 nm (CSS), respectively (see Figure 3C). The PL spectra for DX MG/CSS/AF show two superimposed peaks due to MEH-PPV and AF. The maximum at 547 nm is due to AF. We investigated the effect of CSS concentration on the intensity of this peak (i.e., $I_{547}$) using the Stern−Volmer equation (see Figure S4). The data indicate quenching of the AF signal due to the CSS particles via NRET occurred within the gel. On the basis of $R_o$ for related fluorophores,[52,53] the present data imply that AF and the polymer dots in CSS had an average separation in the 5−10 nm range.

Parts D and E of Figure 3 show the results of live/dead assays, carried out using human nucleus pulposus (NP) cells, in the presence and absence, respectively, of DXMG/CSS/AF. These images show that cells cultured for up to 72 h did indeed survive in the presence of the gels and remained viable (see also Figure S5). This conclusion is also supported by the Presto Blue assay (Figure S6), which shows that, although there was a small decrease in cell viability after 72 h, approximately 80% of the cells were still viable, when compared to the control. We measured the mechanical properties of the DX MG/CSS/AF gels using uniaxial compression (see Figure 3F), because related gels have been used to support load in degenerated IVDs.[20] The gel had a modulus of 61.4 ± 0.5 kPa and was able to withstand approximately 83.0 ± 1.5% compression before failing with a stress-at-break of 554 ± 5 kPa. These values are in the region where use to augment or repair a degenerated IVD could be considered.[54]

We next investigated the effect of pH on the PL response for the DX MG/CSS/AF gels. The gels swelled strongly when the pH increased (see Figure 4A). The data in Figure 4B show that the emission from the MEH-PPV (∼590 nm) was dominant in the spectrum at pH 4.0. As the pH increased, the AF peak (547 nm) became more pronounced relative to the MEH-PPV peak, although both PL intensities decreased because of gel swelling.

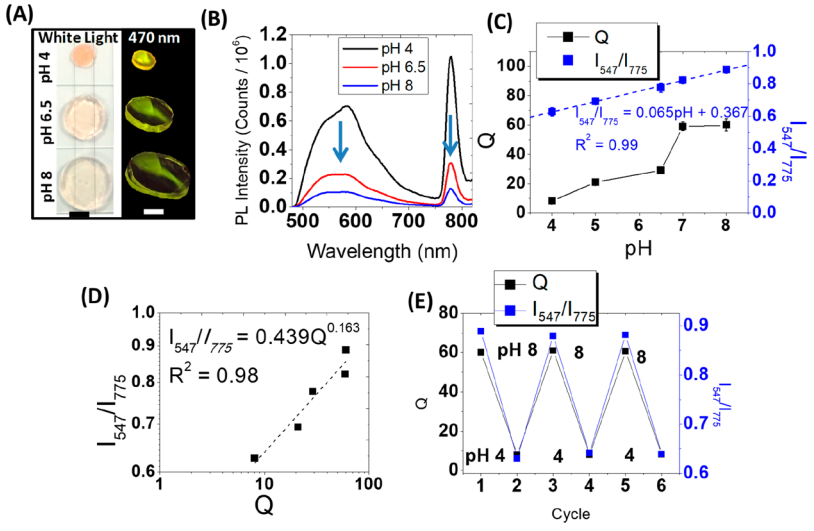


**Figure 4.** (A) Digital photographs of the DX MG/CSS/AF gels under white light (left) and 470 nm light (right). (B) pH-triggered PL changes for DXMG/CSS/AF gel. The PL intensity decreases with increasing pH. (C) $Q$ values as well as the ratio of the PL intensities of the AF peak (547 nm) to the NIR (775 nm) peak over a range of pH values. (D) Double logarithmic plot of the variation of $I_{547}/I_{775}$ with $Q$. (E) Reversibility of $Q$ and the ratiometric PL intensity to pH switching.



DOI: 10.1021/acs.biomac.9b00463
Biomacromolecules 2019, 20, 2694−2702

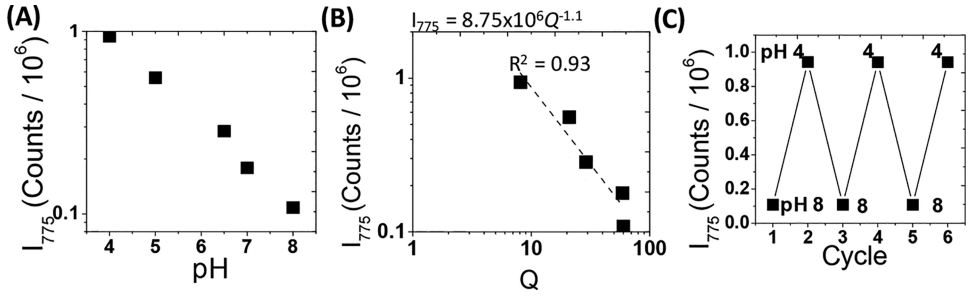


**Figure 5.** (A) Variation of NIR peak PL intensity measured for DX MG/CSS/AF gel with pH. (B) Variation of NIR peak PL intensity for the gel with $Q$. (C) Reversibility of gel NIR PL intensity with pH. The respective $Q$ values are shown in Figure 4E. The spectra are shown in Figure S7.

The relative change of these PL intensities implies that NRET was weakest at pH 8.0. This is due to an increase in distance between the AF donor and MEH-PPV acceptor. The latter was located in the polymer dots within the CSS particles[32] (see Scheme 1). The 547 and 775 nm peak intensities for DX MG/CSS and DX MG/CSS/AF are shown in Table S1. It is noted that DX MG/CSS/AF has greater PL intensities at both wavelengths, across all three pH values compared to DX MG/CSS even though the CSS concentrations were the same in both cases. We followed the energy transfer using the $I_{547}/I_{775}$ ratio. Energy transfer decreased with increasing $I_{547}/I_{775}$. Interestingly, the latter increased linearly with pH (see Figure 4C). Also, a power-law relationship was apparent between $I_{547}/I_{775}$ and $Q$ (see Figure 4D). These data confirm that quenching due to NRET becomes less efficient as $Q$ increases. The $I_{547}/I_{775}$ ratio faithfully tracked the reversible gel swelling/deswelling cycles (see Figure 4E), which is potentially important for applications. The individual spectra of the gels cycled between pH 8 and 4 are shown in Figure S7.

The ability to use NIR emission to monitor swelling is highly desirable because of its relatively high penetration depth through human tissue.[55] We therefore investigated whether NIR intensity alone could be used to follow the changes in swelling caused by pH variation for these gels. The variation of the PL intensity at 775 nm is plotted in Figure 5A as a function of pH, and it can be seen that the intensity of the NIR peak decreases with increasing pH. A similar behavior was apparent for the DX MG/CSS gel above (Figure 2D). In addition, $I_{775}$ showed a negative power-law dependence with $Q$ (see Figure 5B) with an exponent of approximately −1.1. One would expect an inverse relationship between PL intensity and $Q$ if the PL intensity change was solely due to changes in concentration, as suggested by a reviewer. However, the additional effect of decreased NRET has further decreased the exponent to −1.1. In both cases, the cause for this behavior is the decrease of the local CSS concentration caused by swelling, as discussed above. The high correlation of $I_{775}$ with $Q$ indicates good potential for monitoring swelling injectable gel swelling changes remotely using NIR light. Furthermore, the NIR intensity variation with pH shows excellent reversibility (Figure 5C.). Hence, DX MG/CSS/AF, which employed *both* the CSS and AF fluorophores, provides ratiometric *and* single intensity NIR monitoring of gel swelling.

The fact that the PL changes with changes in $Q$ were reversible shows that that AF was not released from the gel (Figure 4E and Figure S7) and suggests that AF was covalently bonded to the gel. The data show that AF did not diffuse away and provide encouragement that AF would may remain in the gel if it were used in vivo. NHS-esters react with nucleophiles, and amines are often used.[56] While DX MG/CSS does not contain amines, every GMA group incorporated provided a hydroxyl group (see Scheme 1). Indeed, a coupling reaction of NHS-esters with hydroxyl groups at pH less than 7 is known.[57] Because the DX MG gels were prepared at pH 6.5, such a coupling reaction between AF and the DX MG matrix is plausible and may account for the reversible PL vs $Q$ changes observed.

In order to demonstrate versatility of our approach, a different, potentially implantable, hydrogel was investigated. PAAm-AA-mBAAm gels are easily prepared and have been used for biological applications such as breast implants and drug delivery.[58,59] Compression data were obtained for PAAm-AA-mBAAm/CSS/AF (Figure S8A). The modulus was 13.8 ± 1.5 kPa, and the strain-at-break was 76.6 ± 3.4% strain. The swelling of the gel was pH dependent and strongly affected the PL spectra (Figure S8B). As the pH increased from pH 2.0 to pH 8.0, $Q$ increased from 7.2 to 51.2 (Figure S8C) and the PL intensity across the whole wavelength range decreased. The value for $I_{547}/I_{775}$ increased linearly with pH (Figure S8C). Furthermore, $I_{547}/I_{775}$ followed a power-law relationship with $Q$ (Figure S8D). The NIR PL peak intensity could also be used to follow the variation of pH and $Q$, as shown in Figure S8E and F, respectively. Hence, including CSS and AF within an implantable gel demonstrated generality of our approach for monitoring gel swelling remotely using *both* ratiometric and single intensity NIR PL measurements. The fact that these gels are also load-bearing suggests that they have potential future applications in vivo, such as augmentation of degenerated IVDs.

**NIR Imaging of an Injected DX MG/CSS/AF Gel.** Finally, we investigated the ability to use DX MG/CSS/AF as an injectable gel for NIR imaging. Figure 6A shows that the precursor dispersion emitted NIR light when irradiated at 470 nm. This was due to a combination of NIR emission and Tyndall scattering. Parts B and C of Figure 6 show white light and NIR imaging of the gel when injected into a chicken breast, at a depth of ∼2.0 mm. The wavelength of 470 nm resulted in maximum fluorescence of the gel and caused minimal NIR autofluorescence of the chicken breast. The use of 470 nm wavelength also enabled internal energy transfer to the NIR775 emission. It can be seen from Figure 6C that the injected gel had a higher NIR fluorescence intensity when compared to the plain chicken breast. A control (DX MG gel) that did not contain fluorophores was also placed on the surface of the chicken flesh. The latter sample resulted in no fluorescence. DX MG/CSS/AF gel was also injected onto the surface of the chicken for comparison, and this could easily be seen via the NIR camera. These data demonstrate that


DOI: 10.1021/acs.biomac.9b00463
*Biomacromolecules* 2019, 20, 2694−2702

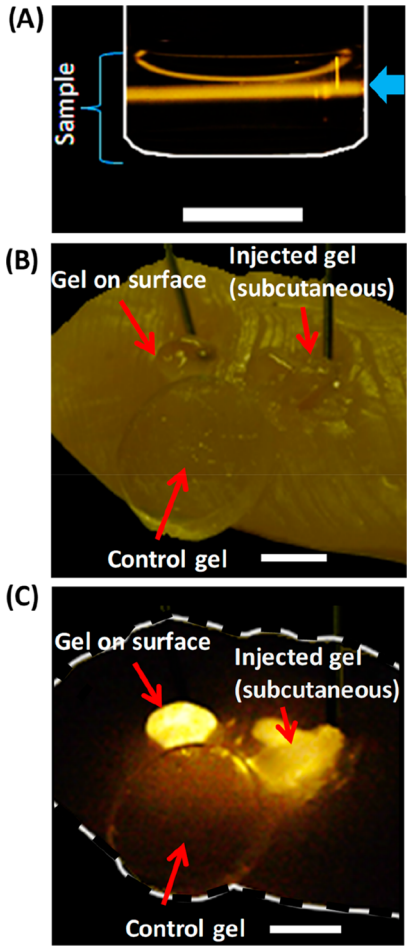


**Figure 6.** Digital photographs showing (A) a mixed MG/CSS/AF dispersion before curing. NIR imaging of the chicken breast was undertaken with subcutaneous DXMG injection, at a depth of 2 mm, when irradiated with a 470 nm laser. The blue arrow represents the incident irradiation beam. The white outline represents the sides of the vial. After subcutaneous injection of gel, the NIR fluorescence intensity increased. The system is shown with a sample of the DX MG/CSS/AF gel and a control gel which did not contain fluorophores (DX MG) on top of the flesh. Part B shows the system in white light. Part C shows NIR light emitted by the DX MG/CSS/AF gel (≥720 nm), when it has been excited with 470 nm light. The chicken breast is outlined. Scale bars: 5.0 mm.

injectable DX MG/CSS/AF gel has good potential for NIR imaging. A potential limitation of NIR imaging using an excitation wavelength of 470 nm is that it only has an epidermis penetration depth of approximately 0.3 mm.[60]

## CONCLUSIONS

In this study, new CSS nanoparticles were used to image gels and monitor changes in swelling using NIR light. The use of added AF dye enabled ratiometric detection to be used. In our approach, the CSS and AF dye were simply blended with the gel precursors. Inclusion of the low concentrations of CSS particles did not alter the swelling properties of the DX MG gels. The injectable pH-responsive gels studied here reversibly swelled when the pH was changed between 4.0 and 8.0. The AF-containing gels were able to sensitively report the swelling changes due to NRET. The CSS particles also enabled the gels to be studied using exclusively NIR emission, which has added potential for future biomaterial applications. We also demonstrated the versatility of this new approach to NIR labeling via CSS particle entrapment by using it for a model implantable PAAm-AA-mBAAm gel. The data reported in this work bring the possibility of injectable NIR gels that have potential for both imaging and remote monitoring of swelling and load support for DIVDs a step closer.

## ASSOCIATED CONTENT

### Supporting Information

The Supporting Information is available free of charge on the ACS Publications website at DOI: 10.1021/acs.biomac.9b00463.

UV and PL spectra with the pH invariance of CSS particles, titration and DLS data, UV and PL spectra for AF and CSS solutions including the spectra overlap of AF emission and CSS absorbance, PL spectra for DX MG/CSS/AF gels with varying CSS concentrations, live/dead images, cycled PL spectra, and mechanical properties and fluorescent data for PAAm-AA/CSS/AF gel as well as a table of PL intensities for DX MG/CSS and DX MG/CSS/AF (PDF)

## AUTHOR INFORMATION

### Corresponding Authors

*E-mail: hannah.shanks@postgrad.manchester.ac.uk.
*E-mail: brian.saunders@manchester.ac.uk.

### ORCID

Hannah R. Shanks: 0000-0002-4952-8493
Brian R. Saunders: 0000-0003-1410-2967

### Notes

The authors declare no competing financial interest.

## ACKNOWLEDGMENTS

This work was supported by a 5-year EPSRC Established Career Fellowship awarded to B.R.S. (EP/M002020/1). The authors also thank the staff in the EM Core Facility in the Faculty of Biology, Medicine and Health for their assistance and the Welcome Trust for equipment grant support to the EM Core Facility. We would like to thank one of the reviewers for their helpful and insightful comments regarding this manuscript.

## REFERENCES

(1) Fraylich, M. R.; Liu, R.; Richardson, S. M.; Baird, P.; Hoyland, J.; Freemont, A. J.; Alexander, C.; Shakesheff, K.; Cellesi, F.; Saunders, B. R. Thermally-triggered gelation of PLGA dispersions: Towards an injectable colloidal cell delivery system. *J. Colloid Interface Sci.* **2010**, *344*, 61−69.
(2) Yu, L.; Ding, J. Injectable hydrogels as unique biomedical materials. *Chem. Soc. Rev.* **2008**, *37*, 1473−1481.
(3) Burdick, J. A.; Anseth, K. S. Photoencapsulation of osteoblasts in injectable RGD-modified PEG hydrogels for bone tissue engineering. *Biomaterials* **2002**, *23*, 4315−23.
(4) Koutsopoulos, S.; Unsworth, L.; Nagai, Y.; Zhang, S. Controlled release of functional proteins through designer self-assembling peptide nanofiber hydrogel scaffold. *Proc. Natl. Acad. Sci. U. S. A.* **2009**, *106*, 4623−8.
(5) Guvendiren, M.; Lu, H. D.; Burdick, J. A. Shear-thinning hydrogels for biomedical applications. *Soft Matter* **2012**, *8*, 260−272.
(6) Sivakumaran, D.; Maitland, D.; Hoare, T. Injectable Microgel-Hydrogel Composites for Prolonged Small-Molecule Drug Delivery. *Biomacromolecules* **2011**, *12*, 4112−4120.



DOI: 10.1021/acs.biomac.9b00463
*Biomacromolecules* 2019, 20, 2694−2702

(7) Bakaic, E.; Smeets, N. M. B.; Badv, M.; Dodd, M.; Barrigar, O.; Siebers, E.; Lawlor, M.; Sheardown, H.; Hoare, T. Injectable and Degradable Poly(Oligoethylene glycol methacrylate) Hydrogels with Tunable Charge Densities as Adhesive Peptide-Free Cell Scaffolds. *ACS Biomater. Sci. Eng.* **2018**, *4*, 3713−3725.
(8) Lee, J. H. Injectable hydrogels delivering therapeutic agents for disease treatment and tissue engineering. *Biomater. Res.* **2018**, *22*, 27.
(9) Hasan, M. D. A.; Khattab, A.; Islam, M.; Abou Hweij, K.; Zeitouny, J.; Waters, R.; Sayegh, M.; Monowar Hossain, M.; Paul, A. Injectable Hydrogels for Cardiac Tissue Repair after Myocardial Infarction. *Adv. Sci.* **2015**, *2*, 1500122.
(10) Mauri, E.; Negri, A.; Rebellato, E.; Masi, M.; Perale, G.; Rossi, F. Hydrogel-Nanoparticles Composite System for Controlled Drug Delivery. *Gels* **2018**, *4*, 74.
(11) Ivashkov, O. V.; Yakimova, T. M.; Evtushenko, E. G.; Gelissen, A. P. H.; Plamper, F. A.; Richtering, W.; Yaroslavov, A. A. On the mechanism of payload release from liposomes bound to temperature-sensitive microgel particles. *Colloids Surf., A* **2019**, *570*, 396−402.
(12) Ko, D. Y.; Shinde, U.; Yeon, B.; Jeong, B. Recent progress of in situ formed gels for biomedical applications. *Prog. Polym. Sci.* **2013**, *38*, 672−701.
(13) Griffin, D. R.; Weaver, W. M.; Scumpia, P. O.; Di Carlo, D.; Segura, T. Accelerated wound healing by injectable microporous gel scaffolds assembled from annealed building blocks. *Nat. Mater.* **2015**, *14*, 737.
(14) Nagahama, K.; Oyama, N.; Ono, K.; Hotta, A.; Kawauchi, K.; Nishikata, T. Nanocomposite injectable gels capable of self-replenishing regenerative extracellular microenvironments for in vivo tissue engineering. *Biomater. Sci.* **2018**, *6*, 550−561.
(15) Hong, J. H.; Lee, H. J.; Jeong, B. Injectable Polypeptide Thermogel as a Tissue Engineering System for Hepatogenic Differentiation of Tonsil-Derived Mesenchymal Stem Cells. *ACS Appl. Mater. Interfaces* **2017**, *9*, 11568−11576.
(16) Doench, I.; Torres-Ramos, M. E. W.; Montembault, A.; Nunes de Oliveira, P.; Halimi, C.; Viguier, E.; Heux, L.; Siadous, R.; Thiré, R. M. S. M.; Osorio-Madrazo, A. Injectable and Gellable Chitosan Formulations Filled with Cellulose Nanofibers for Intervertebral Disc Tissue Engineering. *Polymers* **2018**, *10*, 1202.
(17) Pérez-San Vicente, A.; Peroglio, M.; Ernst, M.; Casuso, P.; Loinaz, I.; Grande, H.-J.; Alini, M.; Eglin, D.; Dupin, D. Self-Healing Dynamic Hydrogel as Injectable Shock-Absorbing Artificial Nucleus Pulposus. *Biomacromolecules* **2017**, *18*, 2360−2370.
(18) Hoemann, C.; Sun, J.; Légaré, A.; McKee, M.; Buschmann, M. Tissue engineering of cartilage using an injectable and adhesive chitosan-based cell-delivery vehicle. *Osteoarthritis Cartilage* **2005**, *13*, 318−29.
(19) Freemont, T. J.; Saunders, B. R. pH-Responsive microgel dispersions for repairing damaged load-bearing soft tissue. *Soft Matter* **2008**, *4*, 919−924.
(20) Milani, A. H.; Freemont, A. J.; Hoyland, J. A.; Adlam, D. J.; Saunders, B. R. Injectable doubly cross-linked microgels for improving the mechanical properties of degenerated intervertebral discs. *Biomacromolecules* **2012**, *13*, 2793−801.
(21) Drake, R. L.; Vogl, W.; Mitchell, A. W. M.; Gray, H. *Gray's Anatomy for Students*; Churchill Livingstone/Elsevier: Philadelphia, 2015.
(22) Liem, K. F.; Walker, W. F. *Functional anatomy of the vertebrates: an evolutionary perspective*; Harcourt College Publishers: Fort Worth, TX, 2001.
(23) Netter, F. H. *Atlas of human anatomy*; Saunders/Elsevier: Philadelphia, PA, 2006.
(24) Roberts, S.; Evans, H.; Trivedi, J.; Menage, J. Histology and pathology of the human intervertebral disc. *J. Bone Jt. Surg., Am.* **2006**, *88*, 10−14.
(25) Pennicooke, B.; Hussain, I.; Berlin, C.; Sloan, S. R.; Borde, B.; Moriguchi, Y.; Lang, G.; Navarro-Ramirez, R.; Cheetham, J.; Bonassar, L. J.; Härtl, R. Annulus Fibrosus Repair Using High-Density Collagen Gel: An In Vivo Ovine Model. *Spine* **2017**, *43*, E208−E215.
(26) Priyadarshani, P.; Li, Y.; Yang, S.; Yao, L. Injectable hydrogel provides growth-permissive environment for human nucleus pulposus cells. *J. Biomed. Mater. Res., Part A* **2016**, *104*, 419−426.
(27) Ntziachristos, V.; Bremer, C.; Weissleder, R. Fluorescence imaging with near-infrared light: new technological advances that enable in vivo molecular imaging. *Eur. J. Radiol.* **2003**, *13*, 195−208.
(28) Avci, P.; Gupta, A.; Sadasivam, M.; Vecchio, D.; Pam, Z.; Pam, N.; Hamblin, M. R. Low-level laser (light) therapy (LLLT) in skin: stimulating, healing, restoring. *Semin. Cutaneous Med. Surg.* **2013**, *32*, 41−52.
(29) Noh, Y.-W.; Kong, S.-H.; Choi, D.-Y.; Park, H. S.; Yang, H.-K.; Lee, H.-J.; Kim, H. C.; Kang, K. W.; Sung, M.-H.; Lim, Y. T. Near-Infrared Emitting Polymer Nanogels for Efficient Sentinel Lymph Node Mapping. *ACS Nano* **2012**, *6*, 7820−7831.
(30) Qin, X.-H.; Wang, X.; Rottmar, M.; Nelson, B. J.; Maniura-Weber, K. Near-Infrared Light-Sensitive Polyvinyl Alcohol Hydrogel Photoresist for Spatiotemporal Control of Cell-Instructive 3D Microenvironments. *Adv. Mater.* **2018**, *30*, 1705564.
(31) Tong, X.; Xiang, J.; Shi, F.; Zhao, Y. Near-Infrared Light-Sensitive Supramolecular Gel with Enhanced Visible Light Upconversion. *Adv. Opt. Mater.* **2016**, *4*, 1392−1396.
(32) Shanks, H. R.; Zhu, M.; Milani, A. H.; Turton, J.; Haigh, S.; Hodson, N. W.; Adlam, D.; Hoyland, J.; Freemont, T.; Saunders, B. R. Core−shell−shell cytocompatible polymer dot-based particles with near-infrared emission and enhanced dispersion stability. *Chem. Commun.* **2018**, *54*, 9364−9367.
(33) Richtering, W.; Saunders, B. R. Gel architectures and their complexity. *Soft Matter* **2014**, *10*, 3695−3702.
(34) Gong, J. P. Why are double network hydrogels so tough? *Soft Matter* **2010**, *6*, 2583−2590.
(35) Jones, C. D.; Lyon, L. A. Synthesis and Characterization of Multiresponsive Core−Shell Microgels. *Macromolecules* **2000**, *33*, 8301−8306.
(36) Dai, S.; Ravi, P.; Tam, K. C. pH-Responsive polymers: synthesis, properties and applications. *Soft Matter* **2008**, *4*, 435−449.
(37) Ballauff, M.; Lu, Y. Smart" nanoparticles: Preparation, characterization and applications. *Polymer* **2007**, *48*, 1815−1823.
(38) Amalvy, J. I.; Wanless, E. J.; Li, Y.; Michailidou, V.; Armes, S. P.; Duccini, Y. Synthesis and Characterization of Novel pH-Responsive Microgels Based on Tertiary Amine Methacrylates. *Langmuir* **2004**, *20*, 8992−8999.
(39) Bysell, H.; Widenbring, R.; Hansson, P.; Malmsten, M. Microgels and microcapsules in peptide and protein drug delivery. *Adv. Drug Delivery Rev.* **2011**, *63*, 1172−85.
(40) Lapeyre, V.; Renaudie, N.; Dechezelles, J.-F.; Saadaoui, H.; Ravaine, S.; Ravaine, V. Multiresponsive Hybrid Microgels and Hollow Capsules with a Layered Structure. *Langmuir* **2009**, *25*, 4659−4667.
(41) Liu, R.; Milani, A. H.; Freemont, T. J.; Saunders, B. R. Doubly crosslinked pH-responsive microgels prepared by particle interpenetration: swelling and mechanical properties. *Soft Matter* **2011**, *7*, 4696−4704.
(42) Echeverria, C.; Fernandes, S. N.; Godinho, M. H.; Borges, J. P.; Soares, P. I. P. Functional Stimuli-Responsive Gels: Hydrogels and Microgels. *Gels* **2018**, *4*, 54.
(43) Backes, S.; Von Klitzing, R. Nanomechanics and Nanorheology of Microgels at Interfaces. *Polymers* **2018**, *10*, 978.
(44) Wu, P. G.; Brand, L. Resonance Energy Transfer: Methods and Applications. *Anal. Biochem.* **1994**, *218*, 1−13.
(45) Yun, C. S.; Javier, A.; Jennings, T.; Fisher, M.; Hira, S.; Peterson, S.; Hopkins, B.; Reich, N. O.; Strouse, G. F. Nanometal Surface Energy Transfer in Optical Rulers, Breaking the FRET Barrier. *J. Am. Chem. Soc.* **2005**, *127*, 3115−3119.
(46) Lakowicz, J. *Principles of Fluorescence Spectroscopy*; Springer: USA, 2006; Vol. *1*.
(47) Smith, G. L.; McCormick, C. L. Water-Soluble Polymers. 78. Viscosity and NRET Fluorescence Studies of pH-Responsive Twin-Tailed Associative Terpolymers Based on Acrylic Acid and Methacrylamide. *Macromolecules* **2001**, *34*, 918−924.


DOI: 10.1021/acs.biomac.9b00463
*Biomacromolecules* 2019, 20, 2694−2702

(48) Xiong, L.; Guo, Y.; Zhang, Y.; Cao, F. Highly luminescent and photostable near-infrared fluorescent polymer dots for long-term tumor cell tracking in vivo. *J. Mater. Chem. B* **2016**, *4*, 202−206.
(49) Cui, Z.; Wang, W.; Obeng, M.; Chen, M.; Wu, S.; Kinloch, I.; Saunders, B. R. Using intra-microgel crosslinking to control the mechanical properties of doubly crosslinked microgels. *Soft Matter* **2016**, *12*, 6985−6994.
(50) Nesrinne, S.; Djamel, A. Synthesis, characterization and rheological behavior of pH sensitive poly(acrylamide-co-acrylic acid) hydrogels. *Arabian J. Chem.* **2017**, *10*, 539−547.
(51) Sun, J.; Ling, P.; Gao, F. A Mitochondria-Targeted Ratiometric Biosensor for pH Monitoring and Imaging in Living Cells with Congo-Red-Functionalized Dual-Emission Semiconducting Polymer Dots. *Anal. Chem.* **2017**, *89*, 11703−11710.
(52) Wiederschain, G. Y. Membrane protein structure determination. Methods and protocols. *Biochemistry* **2011**, *76*, 1277−1277.
(53) Johnson, I. D. *Molecular Probes Handbook: A Guide to Fluorescent Probes and Labeling Technologies*; Life Technologies Corporation: 2010.
(54) Cloyd, J. M.; Malhotra, N. R.; Weng, L.; Chen, W.; Mauck, R. L.; Elliott, D. M. Material properties in unconfined compression of human nucleus pulposus, injectable hyaluronic acid-based hydrogels and tissue engineering scaffolds. *Eur. Spine J.* **2007**, *16*, 1892−1898.
(55) Weissleder, R. A clearer vision for in vivo imaging. *Nat. Biotechnol.* **2001**, *19*, 316.
(56) Kalkhof, S.; Sinz, A. Chances and pitfalls of chemical cross-linking with amine-reactive N-hydroxysuccinimide esters. *Anal. Bioanal. Chem.* **2008**, *392*, 305−12.
(57) Leavell, M. D.; Novak, P.; Behrens, C. R.; Schoeniger, J. S.; Kruppa, G. H. Strategy for selective chemical cross-linking of tyrosine and lysine residues. *J. Am. Soc. Mass Spectrom.* **2004**, *15*, 1604−11.
(58) Ramkissoon-Ganorkar, C.; Liu, F.; Baudyš, M.; Kim, S. W. Modulating insulin-release profile from pH/thermosensitive polymeric beads through polymer molecular weight. *J. Controlled Release* **1999**, *59*, 287−298.
(59) Unukovych, D.; Khrapach, V.; Wickman, M.; Liljegren, A.; Mishalov, V.; Patlazhan, G.; Sandelin, K. Polyacrylamide Gel Injections for Breast Augmentation: Management of Complications in 106 Patients, a Multicenter Study. *World J. Surg.* **2012**, *36*, 695−701.
(60) Avci, P.; Gupta, A.; Sadasivam, M.; Vecchio, D.; Pam, Z.; Pam, N.; Hamblin, M. R. Low-level laser (light) therapy (LLLT) in skin: stimulating, healing, restoring. *Semin. Cutaneous Med. Surg.* **2013**, *32*, 41−52.


DOI: 10.1021/acs.biomac.9b00463
*Biomacromolecules* 2019, 20, 2694−2702